

2021-05

Complex relationships between water discharge and sediment concentration across the Loess Plateau, China

Zheng, H

<http://hdl.handle.net/10026.1/17644>

10.1016/j.jhydrol.2021.126078

Journal of Hydrology

Elsevier BV

All content in PEARL is protected by copyright law. Author manuscripts are made available in accordance with publisher policies. Please cite only the published version using the details provided on the item record or document. In the absence of an open licence (e.g. Creative Commons), permissions for further reuse of content should be sought from the publisher or author.

**Complex relationships between water discharge and sediment
concentration across the Loess Plateau, China**

Haiyan Zheng¹, Chiyuan Miao¹, Juying Jiao^{2, 3}, Alistair G.L. Borthwick⁴

¹ State Key Laboratory of Earth Surface Processes and Resource Ecology, Faculty of
Geographical Science, Beijing Normal University, Beijing 100875, China

² Institute of Soil and Water Conservation, Northwest A&F University, Yangling 712100,
Shaanxi, China

³ Institute of Soil and Water Conservation, Chinese Academy of Sciences and Ministry
of Water Resources, Yangling 712100, Shaanxi, China

⁴ School of Engineering, The University of Edinburgh, The King's Buildings,
Edinburgh EH9 3JL, UK

* Corresponding author. Chiyuan Miao (miaocy@vip.sina.com)

Abstract

Understanding the relationship between water discharge (Q) and suspended sediment concentration (SSC) across the Loess Plateau is a prerequisite for evaluating soil and water conservation measures. Using daily Q and SSC datasets, this study jointly analyzes changes in Q and SSC on the central Loess Plateau, a major sediment-producing area of China, during the periods 1971–1987 (P1) and 2008–2016 (P2). The results show that during both P1 and P2, the contribution of the maximum-3-day-per-year sediment load to the total annual sediment load (SSL) is almost invariably over 50% (dominant), and in the majority of cases, the size of this contribution increases further between P1 and P2. The contribution of extremely high SSL events plays an overwhelming role in watersheds of area $< 10,000 \text{ km}^2$ and appears to be almost independent of change in land cover condition. In the Helong section of the Yellow River, there is more evident reduction in SSC than Q between these two periods (streamflow became clearer), while the opposite occurred in the Jing River (streamflow declined). In addition, the range of variation in SSC is large for small Q values, whereas the SSC for flood events tends to be relatively stable in gullied-hilly and flat-surfaced (*Yuan*) loess areas, which are major sediment producers. Based on scatter plots of SSC versus Q after logarithmic transformation, we find that the lower boundary of the mapped data points for an individual station fits a straight line. This boundary relates to riverbed erosion. Given that soil erosion weakened on gully slopes over time and streamflow in channels during P2 was generally lower, the boundary tended to move downward between P1 and P2 for most watersheds, reflecting a reduction in SSC for a

41 given value of Q in P2 compared to P1.

42

43 **Key words:**

44 Loess Plateau; Extremely high *SSL* events; Discharge–sediment relationship; Stable

45 sediment concentration; Sediment carrying capacity;

46

1 Introduction

The relationship between discharge and sediment load poses a longstanding key challenge in the field of hydrology, and reflects the characteristics of sediment deposition and transport in rivers (Guan, 1999). Müller and Förstner (1968) reported that the water discharge–sediment concentration relationship of a basin can be expressed by the empirical power function $SSC = a \times Q^b$, where SSC is suspended sediment concentration (kg/m^3), Q is discharge (m^3/s), and a and b are parameters. This has been verified for different basins around the world, including the Colorado River near the Grand Canyon (Gray et al., 2008), the Sukhaya Elizovskaya River (Mouri et al., 2014), the Magdalena River (Higgins et al., 2016), and the Ceyhan River Basin (Yüce et al., 2018). However, the discharge–sediment relationship varies across space and time and is vulnerable to human activities (e.g. land use change and soil and water conservation engineering measures) and unexpected events (e.g. landslide and hillslope collapse); this makes development of accurate simulations challenging. Consequently, in addition to conventional statistical methods, new methods, such as artificial neural networks (Yang et al., 2009) and Gaussian mixture modeling (Gournelos et al., 2020), have been developed and applied in the study of discharge–sediment relationships.

The Loess Plateau, located in northern China, contains the middle Yellow River. This region is famous for its severe soil erosion and complex discharge–sediment relationships. To control soil erosion and prevent sediment from entering the Yellow River, many large-scale soil and water conservation projects were introduced starting in the 1970s, followed by ecological projects from 1999 onwards. These projects

69 profoundly changed conditions on the plateau and greatly altered the complex
70 discharge–sediment relationships (Zhang et al., 2017; Zhao et al., 2012). Researchers
71 have devoted much effort to trying to model these relationships and hence interpret their
72 temporal variation (Wang et al., 2007; Zhao et al., 2017; Zheng et al., 2020). Using a
73 monthly dataset for 14 watersheds and a daily dataset for 9 watersheds on the Loess
74 Plateau, Gao et al. (2018) proposed a generalized power-law sediment rating curve by
75 which to describe the daily water discharge–sediment relationship, and linear functions
76 for annual and monthly discharge–sediment relationships. Using a daily Q and SSC
77 dataset for the Beiluo River basin, Zhang et al. (2017) demonstrated that the streamflow
78 and the discharge–sediment relationship both changed due to recent ecological
79 restoration measures. In the context of climate change (Gou et al., 2019; Sun et al.,
80 2019), extremely intense hydrological events have always been a major concern
81 regarding sediment flux. Previous researchers reported that the decrease in SSL is
82 mainly caused by the changing discharge–sediment relationship during flood events,
83 whereas the relationship for relatively small values of Q involves only limited change
84 (Liao et al., 2008; Rustomji et al., 2008; Xu, 2002). However, Zheng et al. (2007)
85 reported that the SSC in certain small watersheds in gullied-hilly areas remained
86 relatively stable under heavy storms and changes in area of vegetation cover did not
87 alter the discharge–sediment relationship. The foregoing leads us to speculate about the
88 change in discharge–sediment relationship that occurs between extreme and ordinary Q
89 events, separate from the degree of change in Q and SSC .

90 In this study, we analyze changes in the SSC – Q relationship for the major

sediment-producing area of the Loess Plateau. Specifically, we determine the change in extremely high SSL , compare the degree of change in both Q and SSC , devise expressions for the patterns of change in SSC – Q relationships, and examine the leading reasons behind these changes. An understanding of the change characteristics inherent to the SSC – Q relationship for the Loess Plateau would provide a foundation for optimizing the production and transportation processes affecting streamflow and sediment and for evaluating and hence prioritizing different soil and water conservation measures.

2 Data and Methods

2.1 Study area and dataset

The Loess Plateau of China, a cradle of ancient Chinese civilization, possesses the most concentrated and largest area of loess in the world. It is highly prone to soil erosion, with the most severe areas situated along the Helong section of the Yellow River basin (hereafter, ‘the Helong section’), the Beiluo River, and the Jing River. Taken together, these areas account for about 92% of the total SSL on the Loess Plateau during 1956–2000 (Ran, 2006), even though their total area accounts for just 29% of the total area of the plateau. Changes in SSC – Q in these regions have long been of great concern. Moreover, these regions have a characteristic landscape that produces sediment, called the loess gully area (which includes the loess gullied-hilly areas and the loess *Yuan* areas depicted in Fig. 1). The mean annual sediment yield of the loess gully area reached 10,000 t/km² before 1970 (Gong and Jiang, 1978). In recent years however, soil erosion

in most regions has been successfully controlled through soil management measures (Xin et al, 2009), whereas the discharge–sediment relationship has become more complicated due to human activities.

< Figure 1 >

In the present study, our dataset comprises daily records of Q (m^3/s) and SSC (kg/m^3) acquired at 47 hydrological stations located on the Helong section, the Beiluo River, and the Jing River (Fig. 1) for two periods spanning 1971–1987 (P1 period) and 2008–2016 (P2 period). The data were obtained from the Hydrological Yearbooks of the People’s Republic of China, compiled by the Yellow River Conservancy Commission (<http://www.yellowriver.gov.cn/>). Basic information for the three basins is presented in Fig. S1. The wet season is the most important period for sediment generation and transport in the Yellow River, with nearly 95% of sediment transported from May to October (Zheng et al., 2019). Taking the integrity of the dataset into account, also, we only use wet-season data (which is quite complete) to analyze changes in the SSC – Q relationship.

2.2 Methods

2.2.1 Quantifying the contribution of SSC to changes in SSL

It is of interest to know whether Q or SSC plays the bigger role in the observed sediment load changes between periods P1 and P2. To determine this, we use a simple

method that first divides the daily SSC by the daily Q to give the daily SSC/Q ratio. Then, we calculate the mean value and the standard deviation (std) of SSC/Q sequence values in P1 and in P2 and compare them. We pretreat the data by removing daily Q values that are less than $0.01 \text{ m}^3/\text{s}$ and the corresponding SSC values, because for $Q < 0.01 \text{ m}^3/\text{s}$, the resulting value of SSC/Q would be very large and disproportionately influence the mean and std of the SSC/Q values. The number of instances where $Q < 0.01 \text{ m}^3/\text{s}$ accounts for less than 10% of the data for all stations except for two stations in P1 and four stations in P2.

To quantify the contribution of SSC to the change in SSL , we perform an additional set of calculations through matching the probability density function (PDF) curves for discharge. The steps are as follows:

(i) First compress the PDF curves for discharge during the P1 period according to those during P2; that is, reconstruct the Q sequence in P1 (i.e., $Q_{P1,sim}$). Next, calculate the 1st, 2nd, ..., 99th, and 100th percentiles of the Q sequence in P1 and P2, respectively, and then scale these percentile values in P1 according to the corresponding percentiles in P2. Then, 100 scaling factors are obtained as follows:

$$\begin{aligned}
 k_1 &= per^{1st,P2} / per^{1st,P1} \\
 k_2 &= per^{2nd,P2} / per^{2nd,P1} \\
 &\dots \\
 k_{99} &= per^{99th,P2} / per^{99th,P1} \\
 k_{100} &= per^{100th,P2} / per^{100th,P1}
 \end{aligned} \tag{1}$$

where $per^{xth,P1}$ and $per^{xth,P2}$ are the x^{th} percentile of the Q sequence in P1 and P2, and x

= 1, 2, ..., 99, 100. Next, the Q values are scaled between 0 and $per^{1st,P1}$ by k_1 , between $per^{1st,P1}$ and $per^{2nd,P1}$ by k_2 , ..., and between $per^{99th,P1}$ and $per^{100th,P1}$ by k_{100} . This provides a simulated Q sequence for P1 ($Q_{P1,sim}$).

(ii) The portion of change in SSL solely due to SSC change (SSL_{SSC}) is calculated from:

$$SSL_{SSC} = \sum Q_{P1,sim} \cdot SSC_{P1,mat} - \sum Q_{P2} \cdot SSC_{P2} \quad (2)$$

Here, the PDF curve of $Q_{P1,sim}$ is nearly the same as that of Q_{P2} , and SSC_{P2} and Q_{P2} are the observed SSC and corresponding Q during P2. The $SSC_{P1,mat}$ is the matched value of SSC for each interval (step length set to 3) of observation Q in P1 and, for a specific interval, is calculated from:

$$SSC_{P1,mat} = \sum (Q_i \cdot SSC_i) / \sum Q_i \quad (3)$$

where Q_i and SSC_i are the Q and related SSC values in the specific interval, respectively.

(iii) The contribution of SSC to the change in SSL from P1 to P2 is

$$\text{Contribution of } SSC = \frac{SSL_{SSC}}{SSL_{SSC} + SSL_{not}} \quad (4)$$

where SSL_{not} is the SSL under the hypothetical condition that the PDF curves of SSC and Q in P1 are both the same as in P2 (which is equal to the observed SSL during P2). More details about the PDF-matching method and its uncertainty discussion can be found in the supplementary materials.

2.2.2 Estimating the boundaries of numerous scatter plots

From the observed dataset, we find that scatter plots of SSC against Q exhibit distinct areas of concentration for most watersheds. Taking Station 31 as an example

(Fig. 2), we plot lines to fit the upper and lower boundaries of the data to delineate these areas of concentration. The lines show that SSC varies greatly when Q is small, whereas SSC tends to be relatively stable for large Q events (Fig. 2a and b). Next, we consider the change in position of boundary lines between the two periods as reflecting the change in the discharge–sediment relationship (Fig. 2c). We then carry out a logarithmic transformation (using the natural logarithm) on both SSC and Q to further study the changing features of the relationship. We find that a linear equation gives a satisfactory fit to the lower boundary of the logarithmically transformed data points (Fig. 2d and e). Details for estimating the boundaries of the numerous scatter plots follow.

First, the reordered Q sequence is divided into a large number of intervals of fixed step length. Then, the points with smallest or largest SSC are identified in each interval (i.e., the prepared points) and used to fit the boundary using a nonlinear equation (Fig. 2a and b),

$$y = a \cdot \exp^{-\frac{x}{b}} + c \cdot \exp^{-\frac{x}{d}} + e \quad (5)$$

where a , b , c , d , and e are fitting parameters (Fig. 2a and b), and using a linear equation (Fig. 2d and e). To delineate the boundary, we use bootstrap sampling (with drop-back sampling). Specifically, we first randomly pick 75% of the prepared points to fit the boundary. Then we repeat the step 50 times to obtain 50 lower boundaries (Fig. 2d and 2e). To check the effect of sample size on boundary fitting, we also randomly pick 25% and 50% of points to fit the boundary, again repeating 50 times. Fig. S4 presents the results. We find the lower-boundary fitting equations to be robust. In addition, considering that the distribution of observed SSC – Q points is extremely uneven, we fit

the lines using a few larger Q points, so that a single line appears in Fig. 2a and b. More details about the uncertainty analysis and applicability of the method are given in the supplementary material. We call this method ‘Boundary Estimation with Interval Extremum’ (BEIE).

< Figure 2 >

3 Results

3.1 Change in contributions of extremely high *SSL* events to total *SSL*

In this paper, extremely high *SSL* events refer to maximum- n -day-per-year *SSL* events during period P1 or period P2 ($n = 1, 2, \dots, 6$). Fig. 3c shows that contributions of maximum-3-day *SSL* generally exceeded 50% in both P1 and P2. However, compared with P1, most contributions became larger in P2 (the majority of points are above the 1:1 dashed lines), which illustrates that extremely high *SSL* events have played a more important role in recent years and suggests that the effect of soil management measures on extremely high *SSL* events was not as strong as on ordinary *SSL* events. Fig. 4 shows the relationship between the percentage contributions of extreme *SSL* events (occurrence ranging from 1 to 6 days per annum) with the control area of the hydrological stations. Other than for the maximum-1-day *SSL* event (Fig. 4a and g), the contributions of extremely high *SSL* events generally dominate (exceeding 50%) when the watershed area is less than 10,000 km² (see points in the top left quadrant of each graph), and this relationship with watershed area has little to do with

change in land cover conditions. We speculate that when the basin area is larger than a specific threshold value (such as the 10,000 km² value identified in this study), underlying conditions rather than topography might play a more critical role in the sediment load at the outlet of a basin; conversely, the topography determines the extremes for relatively small basins.

< Figure 3 >

< Figure 4 >

3.2 Contribution of *SSC* to the change in *SSL*

Both *SSC* and *Q* decreased in P2 relative to P1. Fig. 5a shows that the average value of *SSC/Q* was almost invariably smaller in P2 than in P1 (except for one outlier), indicating that the reduction in *SSC* was effectively much larger than the reduction in *Q*. Fig. 5b shows that the variability in *SSC/Q* was also much smaller in P2 than in P1 (except for two outliers). Fig. 5 shows that the expected value and variability of *SSC* decreased relative to that of *Q* between periods P1 and P2; this resulted in a significant increase in *SSL*. Generally speaking, sudden gravity erosion events, such as landslide or hillslope collapse, could lead to small *Q* and large *SSC*. Increased frequency of such events could raise the standard deviation of *SSC/Q*.

Then, through quantifying the contribution of *SSC* to the change in *SSL*, we found that the contribution of *SSC* is generally more than 50% for watersheds in the Helong section, whereas the contribution of *SSC* in the Jing River basin is generally less than

50%; this implies that the factor driving the drop in *SSL* is the decline in *SSC* in Helong and the decline in *Q* in the Jing River. This is basically consistent with the results produced using double mass curves (Figs S7 and S8). In addition, Fig. 6 shows that many contribution values are concentrated around 76%. So, in brief, even though both *Q* and *SSC* decreased on the central plateau, the decline in *SSC* is more important than the decrease in *Q*.

< Figure 5 >

< Figure 6 >

3.3 Changes in upper and lower boundaries of *SSC* vs. *Q* scatter plots

Just as at Station 31 (discussed in Section 2.2.2), the *SSC–Q* distributions during the P1 period have distinct areas of concentration for watersheds where gully landforms dominate the control area (Fig. 7). However, this distribution pattern is not common in the more complicated geomorphologic regions (Fig. S6), demonstrating that the pattern correlates closely with geomorphic characteristics. For watersheds dominated by gully landforms, the general trend in the upper boundary line for *SSC* is to decline slightly at first and then stabilize with increasing discharge. By comparison, the trend in the lower boundary is first to increase and then to reach a stable value with greater *Q* values. In other words, *SSC* in larger *Q* events (flood events) remains relatively stable in these watersheds. However, the boundaries of about half of these watersheds are indistinct (*SSC–Q* distribution is irregular) in P2. For the other half of these watersheds, we found

that both boundaries tended to move downward between P1 and P2, except for the Jing River basin.

< Figure 7 >

With respect to the lower boundary, it is obvious that its fit is not very precise because most Q data are concentrated at smaller values, and there is an enormous difference between the smallest and largest values. Given that the lower boundary relates to streamflow erosivity, we carried out log transformations of $SSC-Q$ and then focused on middle and large Q values. With these transformed values, we found that a linear equation can describe the mapped lower boundary well for almost all watersheds (Fig. 8). The lower boundary, corresponding to the smallest SSC in the streamflow, relates to the sediment carrying capacity of the river channels. As Q increases, the scouring capacity of the streamflow is enhanced, and so SSC becomes greater. This process continues until reaching dynamic equilibrium between erosion and deposition, and after that, SSC tends to be stable.

< Figure 8 >

In fact, the upper and lower boundaries are both extreme cases — that is, cases where the SSC on slopes is extremely high or close to zero (i.e., clear runoff). More often, the observed SSC at the watershed outlet lies somewhere between the two

boundaries. And at daily scale, the raw $SSC-Q$ relationship cannot be described by a statistical regression equation for most watersheds.

4 Discussion

4.1 Upper and lower boundaries and stable SSC in the loess gully area

The surface of the loess gullied-hilly area is severely incised due to water erosion, sometimes in combination with wind erosion (Fig. 9). Ravine density can reflect the surface degree of crushing. According to Tian et al. (2013), gully density in the central area of the Helong section is up to 10 km/km^2 , and the density in the central area of the Loess Plateau is generally more than 3.5 km/km^2 . Dense gullies provide key transport and storage conditions for sediment, and so slopes and gullies (or channels) become the two main sources of sediment in such watersheds. The type of soil erosion is mainly raindrop splash erosion and sheet erosion on the tops of slopes, rill erosion on the middle and upper parts of slopes, and gully erosion and gravity erosion on the lower slopes (Zheng et al., 2007). Gravity erosion (such as landslides and avalanches) is one of the most important forms of sediment production on the Loess Plateau, and the sediment from gravity erosion is about 20%–25% of the total sediment production of a watershed (Yang et al., 2011). Gravity erosion provides a large quantity of loose material for water flow, resulting in a generally higher SSC during heavy storms on the central Loess Plateau.

< Figure 9 >

Research by Xu (2004) has revealed that slope–channel systems (i.e., those with vertically differentiated landforms) in the loess gully area have an important influence on the formation of high-concentration flows. Xu suggested a storage–release mechanism through which relatively coarse fractions of sediment are more likely to be temporarily deposited and stored in gully channels when slope runoff is relatively low (for example, as a result of small precipitation events), and the deposited sediments might be then carried away later by the high-concentration runoff when heavy precipitation occurs. Wang et al. (1982) reported that many channels have been cut into bedrock in the gullied-hilly area, and so deposition and erosion occur alternately at different times. In short, severe soil erosion on slopes along with a certain level of sediment storage in channels have together ensured a high sediment yield in the loess gully area.

The sediment carrying capacity of streamflow refers to the amount of sediment transported by the streamflow when the riverbed is in an equilibrium state of erosion and deposition (Xu, 1999). Many factors determine sediment carrying capacity, most notably, drainage characteristics (slope, river length and shape, etc.) and sediment properties. When the sediment transport rate reaches the sediment carrying capacity of the streamflow, the riverbed is in a state of dynamic equilibrium whereby the rate of deposition equals the rate of erosion. Fig. 7 shows that *SSC* in flood discharges tends to be relatively high and stable in these areas. But why does *SSC* remain stable? Fig. 9 provides an illustrative explanation of the stability mechanism for *SSC* change during

storm events in the wet season. For high *SSC* of slope flood runoff, sediment is deposited in channels; whereas for lower *SSC* of slope flood runoff, material previously deposited after erosion in the lower slopes or channels is carried away, thus increasing *SSC* in the channels. Hence, the actual streamflow sediment load always approaches the sediment carrying capacity provided the land surface cover remains essentially unchanged. In other words, the stable *SSC* of slope flood runoff may be considered a proxy for sediment carrying capacity. Given the stable, high values of *SSC* during flood events, the contribution of extremely high *SSL* events to the total *SSL* is usually dominant (i.e., more than 50%) for relatively small, gullied watersheds (Figs. 3 and 4). In general, the value of *SSC* observed at the hydrological station will be above the lower boundary since that the lower boundary represents the fitting relationship between the lowest *SSC* and the corresponding *Q*.

4.2 Effect of land cover on the change in upper and lower boundaries in the loess gully area

Check dams are among the most important types of engineering measures on the Loess Plateau (Li et al., 2019). Check dams are usually small and have limited life span. Their main function is to intercept sediment to create farmland. Check dams promote sediment deposition by intercepting and slowing the discharge (Liu et al., 2018), and thus alter the relationship between water discharge and sediment flux (Zhang et al., 2019). Li and Liu (2018) report that 50,935 check dams had been built in the upper reaches of the Yellow River, above Tongguan station (at the mainstream of the Yellow

River) by 2012 when the average amount of intercepting sediment reached 204 million tons per year. *SSC* reduction is the major reason for the decrease in *SSL* in the Helong section, whereas *Q* reduction drove decreasing *SSL* in the Jing River; this may be due to the much larger number of check dams in the Helong section than in the Jing River (Li and Liu, 2018).

Besides check dams, the main difference between periods P1 and P2 is in land use through implementation of the Grain-for-Green Project on the Loess Plateau. Fig. 10 shows that the cultivated land area shrank notably but grassland and woodland area exhibited large increases. Vegetation cover area on the central plateau, also reflected in the Normalized Difference Vegetation Index (NDVI), increased significantly by P2 (Miao et al., 2012; Zheng et al., 2019). Sloping farmland in this region was largely converted to grassland or shrubland (Yu et al., 2009), which led directly to a great reduction in slope erosion (Dang, 2011; Sheng et al., 2016). The effect of natural vegetation on runoff and sediment flux is profound (Jiao et al., 2012; Yu et al., 2012). Interception of precipitation by vegetation leaves and trunks reduces the kinetic energy of raindrops and weakens soil erosion. Vegetation litter increases surface roughness, thus lowering runoff velocity and volume, increasing infiltration, and reducing sediment lateral transport. Plant roots stabilize the soil structure, raise soil resistivity, increase gully slope stability, and reduce the occurrence frequency of gravity erosion events (Miao et al., 2020). Consequently, an increase in vegetation cover reduces not only the volume and velocity of runoff but also the *SSC*, and it may change sediment deposition in rivers. Given the weaker soil erosion of slopes and the stronger

interception ability of channels (check dams) in P2, the discharge–sediment relationship connects more closely to channel than slope transport processes. A change in the sediment transport processes in channels therefore alters the sediment carrying capacity of the streamflow (Fig. 7).

< Figure 10 >

It is interesting to see a declining trend depicted by the upper boundaries. Even when Q is quite small, the associated observed SSC can be extremely high. This is most likely due to sudden gravity erosion. Furthermore, if antecedent soil moisture starts to be saturated, the soil's resistance to rainfall erosion weakens greatly. Under these conditions, surface soil is prone to gravity erosion (such as landslide or gully slope collapse) during rainfall events and the phenomenon of 'small Q –high SSC ' may occur.

Compared with period P1, the range of variation in SSC is smaller and the SSC – Q distribution seems more irregular in P2. However, the lower boundaries of log-transformed SSC – Q again form distinct lines (Fig. 8) and the boundaries tend to move downward, except for the Jing River. This is the overall consequence of land use change and check dams. Q reduced greatly as grassland and woodland area increased significantly (Zhang et al., 2000). Moreover, the reductions in both Q and SSC may have led to the actual streamflow sediment load being insufficient to reach the sediment carrying capacity. As a result, the phenomenon of unstable SSC was commonplace in many watersheds during P2. Of course, the streamflow may reach a new equilibrium state under changed sediment carrying capacity, reflected by a new stable value for SSC

during P2. Because of the weakening of soil erosion caused by land use and the lowering of streamflow kinetic energy (via velocity and volume) caused by land use and check dams, the upper and lower boundaries of *SSC* generally moved downward (Fig. 7) for most watersheds. Moreover, when insufficient sediment was deposited in a channel, then the *SSC*–*Q* distribution tended to be irregular. However, in the Jing River basin, several stations displayed an upward shift of the linear lower boundaries between P1 and P2 (Fig. 8), and the resulting reduction in *SSL* can be attributed to declining *Q*, not *SSC* (Fig. 6). We may infer that slope erosion in the Jing River basin was still considerable, and sediment deposition on the riverbed was likely to be greater in period P2, because the reduced discharge could not carry away all the sediment from the gully slopes.

5 Conclusions

Based on daily discharge (*Q*) and sediment concentration (*SSC*) data from 47 hydrological stations in the major sediment-producing areas on the Loess Plateau (the Helong section of the Yellow River, the Beiluo River, and the Jing River), this paper has explored joint changes in *Q* and *SSC* from period P1 (1971–1987) to P2 (2008–2016). The results show that during both P1 and P2, the contributions of maximum-3-day-per-year sediment load (*SSL*) to the total *SSL* generally exceeded 50% (dominant), and in the majority of cases, these values become larger by P2. The contribution of extremely high *SSL* events (maximum-*n*-day-per-year *SSL*, $n = 1, 2, \dots, 6$) is generally dominant for watersheds whose area is $< 10,000 \text{ km}^2$; this relationship with watershed

area has little to do with change in land cover conditions. Moreover, to determine whether the streamflow became more dilute (in terms of sediment concentration) or less (in terms of water amount) by P2, we calculate and analyze the degrees of change in both SSC and Q . We find that the degree of reduction in SSC is greater than that of Q for most watersheds (28 out of 47), especially in the Helong section. However, the driving factor behind SSC decline is the decrease in Q for the Jing River basin. Also, we find that the range of variation in SSC for smaller values of Q is large, and SSC during flood events tends to be relatively stable in the loess gullied-hilly and *Yuan* areas. In addition, we investigate a linear equation that can describe quite well the lower boundary of an SSC – Q distribution after logarithmic transformation of each variable; this relationship is likely to be related to riverbed erosion. Given the weakening soil erosion of slopes during P2 and the lower volume and slower streamflow in channels, the boundary lines tended to move downward between the two periods.

Acknowledgements

This research was supported by the National Key Research and Development Program of China (No. 2016YFC0501604), and the National Natural Science Foundation of China (No. 41877155). We are grateful to the Yellow River Conservancy Commission (YRCC) for providing the observed water discharge and sediment load (<http://www.yrcc.gov.cn>) and to China Meteorological Administration (CMA) for providing the precipitation data (<http://data.cma.cn/>).

References:

- Dang, W., 2011. Recycled utilization and model analysis in water and soil loss comprehensive harness on slope farmland of Loess Plateau. *China Water Resources* 16, 51-53.
- Fu, B., Wang, S., Liu, Y., Liu, J., Liang, W., Miao, C., 2017. Hydrogeomorphic ecosystem responses to natural and anthropogenic changes in the Loess Plateau of China. *Annu. Rev. Earth. Planet. Sci.* 45, 223-243. doi: 10.1146/annurev-earth-063016-020552
- Gao, G., Fu, B., Zhang, J., Ma, Y., Sivapalan, M., 2018. Multiscale temporal variability of flow-sediment relationships during the 1950s–2014 in the Loess Plateau, China. *J. Hydro.* 563, 609-619. doi: 10.1016/j.jhydrol.2018.06.044
- Gong, S., Jiang, D., 1978. The soil loss and treatment in a small watershed in loess area in the middle reaches of Yellow River. *Science in China* 6, 671-678.
- Gournelos, T., Kotinas, V., Poulos, S., 2020. Fitting a Gaussian mixture model to bivariate distributions of monthly river flows and suspended sediments. *J. Hydro.* doi: 10.1016/j.jhydrol.2020.125166.
- Gou, J., Miao, C., Duan, Q., Tang, Q., Di, Z., Liao, W., et al., 2019. Sensitivity analysis-based automatic parameter calibration of the variable infiltration capacity (VIC) model for streamflow simulations over China. *Water Resources Research* 56(1). doi: 10.1029/2019WR025968
- Gray, J. R., Simões, F. J., 2008. Estimating sediment discharge. *Sedimentation Engineering—Processes, Measurements, Modeling, and Practice*, Manual 110,

456 1067-1088.

457 Guan, H. 1999. Analysis on rivers discharge sediment correlations in the joint zone
 458 between Qingling mountains and Huanghuai Plain. *Journal of Mountain Science*
 459 17(2), 110-114. doi:10.16089/j.cnki.

460 Higgins, A., Restrepo, J. C., Ortiz, J. C., Pierini, J., Otero, L., 2016. Suspended sediment
 461 transport in the Magdalena River (Colombia, South America): Hydrologic regime,
 462 rating parameters and effective discharge variability. *International Journal of*
 463 *Sediment Research* 31(1), 25-35.

464 Jiao, J., Zhang, Z., Bai, W., Jia, Y., Wang, N., 2012. Assessing the ecological success of
 465 restoration by afforestation on the Chinese Loess Plateau. *Restoration Ecology*
 466 20(2), 240-249. doi: 10.1111/j.1526-100X.2010.00756.x

467 Li, J., Liu, L., 2018. Analysis on the sediment retaining amount by warping dams above
 468 Tongguan section of the Yellow River in recent years. *Yellow River* 40(1), 1-6.

469 Li, J., Liu, Q., Feng, X., Shi, W., Fu, B., Lü, Y., Liu, Y., 2019. The synergistic effects of
 470 afforestation and the construction of check-dams on sediment trapping: Four
 471 decades of evolution on the Loess Plateau, China. *Land Degrad. Dev.* 30(6), 622-
 472 635. doi: 10.1002/ldr.3248

473 Liao, J., Xu, J., Yang, Y., 2008. Study of the spatial differentiation of hyperconcentrated
 474 flows frequency in the Loess Plateau. *Advances in Water Science* 19(2), 160-170.

475 Liu, X., Gao, Y., Ma, S., Dong, G. 2018. Sediment reduction of warping dams and its
 476 timeliness in the Loess Plateau. *Journal of Hydraulic Engineering* 49(2), 145-155.

477 Miao, C., Yang, L., Chen, X., Gao, Y., 2012. The vegetation cover dynamics (1982–

478 2006) in different erosion regions of the Yellow River Basin, China. *Land Degrad.*
 479 *Dev.* 23(1), 62-71. doi: 10.1002/ldr.1050
 480 Miao, C., Zheng, H., Jiao, J., Feng, X., Duan, Q., Mpofu, E., 2020. The changing
 481 relationship between rainfall and surface runoff on the Loess Plateau, China. *J.*
 482 *Geophys. Res.: Atmos.* 125. doi: 10.1029/2019JD032053
 483 Mouri, G., Ros, F. C., Chalov, S., 2014. Characteristics of suspended sediment and river
 484 discharge during the beginning of snowmelt in volcanically active mountainous
 485 environments. *Geomorphology* 213, 266-276. doi:
 486 10.1016/j.geomorph.2014.02.001
 487 Müller, G., Förstner, U., 1968. General relationship between suspended sediment
 488 concentration and water discharge in Alpenrhein and some other rivers. *Nature*
 489 217, 5125, 244-245. doi: 10.1038/217244a0
 490 Ran, D., 2006. Water and sediment variation and ecological protection measures in the
 491 middle reach of the Yellow River. *Resources Science* 28(1), 93-100.
 492 Rustomji, P., Zhang, X., Hairsine, P., Zhang, L., Zhao, J., 2008. River sediment load
 493 and concentration responses to changes in hydrology and catchment management
 494 in the Loess Plateau region of China. *Water Resour. Res.* 44(7). doi:
 495 10.1029/2007WR006656
 496 Sheng, H., Cai, Q., Sun, L., 2016. Impacts of loessial texture on slope erosion. *J. Soil*
 497 *Water Conserv.* 30, 31-35.
 498 Sun, Q., Miao, C., Hanel, M., Borthwick, A. G., Duan, Q., Ji, D., Li, H., 2019. Global
 499 heat stress on health, wildfires, and agricultural crops under different levels of

500 climate warming. *Environment International* 128, 125-136. doi:
 501 10.1016/j.envint.2019.04.025

502 Tian, J., Tang, G., Zhou, Y., Song, X., 2013. Spatial variation of gully density in the
 503 Loess Plateau. *Scientia Geographica Sinica* 33(5), 622-628.

504 Wang, H., Yang, Z., Saito, Y., Liu, J., Sun, X., Wang, Y., 2007. Stepwise decreases of
 505 the Huanghe (Yellow River) sediment load (1950–2005): Impacts of climate
 506 change and human activities. *Global Planet Change* 57(3-4), 331-354. doi:
 507 doi:10.1016/j.gloplacha.2007.01.003

508 Wang, X, Qian, N., Hu, W., 1982. The formation and process of confluence of the flow
 509 with hyperconcentration in the gullied-hilly Loess Plateau areas of the Yellow
 510 River basin. *Shuixuebao* 7, 26-35.

511 Xin, Z., Xu, J., Yu, X., 2009. Temporal and spatial variability of sediment yield on the
 512 Loess Plateau in the past 50 years. *Acta Ecologica Sinica* 29(3), 1129-1139.

513 Xu, J., 1999. Erosion caused by hyperconcentrated flow on the Loess Plateau of China.
 514 *Catena* 36, 1-19.

515 Xu, J., 2002. Influence of human activities on hyperconcentrated flows in the middle
 516 Yellow River. *Scientia Geographica Sinica/Dili Kexue* 22(3), 294-299.

517 Xu, J., 2004. Hyperconcentrated flows in the slope-channel systems in gullied hilly
 518 areas on the loess plateau, China. *Geografiska Annaler: Series A, Physical*
 519 *Geography* 86(4), 349-366.

520 Yang, C., Marsooli, R., Aalami, M. T., 2009. Evaluation of total load sediment transport
 521 formulas using ANN. *International Journal of Sediment Research* 24(3), 274-286.

doi: 10.1016/S1001-6279(10)60003-0.

Yang, J., Yao, W., Ma, X., Shao, H., Wang, L., 2011. Progress of the Gravity Erosion and Sediment Yield Study in the Loess Plateau. *Yellow River* 33(9), 77-79.

Yu, G., Li, Z., Zhang, M., Pei, L., 2012. Mechanisms of soil and water conservation measures regulating gravitational erosion in small watersheds on Loess Plateau. *Acta Pedologica Sinica* 49(4), 646-654.

Yu, X., Zhang, X., Niu, L., Yue, Y., Wu, S., Zhang, M., 2009. Dynamic evolution and driving force analysis of land use/cover change on loess plateau watershed. *Transactions of the Chinese Society of agricultural engineering* 25(7), 219-225.

Yüce, M. İ., Eşit, M., Ercan, B., 2018. A relationship between flow discharge, sediment discharge and sub-basin areas in Ceyhan Catchment.

Zhang, J., Gao, G., Fu, B., Gupta, H.V., 2019. Formulating an elasticity approach to quantify the effects of climate variability and ecological restoration on sediment discharge change in the Loess Plateau, China. *Water Resour. Res.* 55(11), 9604-9622. doi: 10.1029/2019WR025840

Zhang, J., Zhang, X., Li, R., Chen, L., Lin, P., 2017. Did streamflow or suspended sediment concentration changes reduce sediment load in the middle reaches of the Yellow River? *J. Hydrol.* 546, 357-369. doi: 10.1016/j.jhydrol.2017.01.002

Zhang, X., Liu, G., Fu, H., 2000. Soil nitrogen losses of catchment by water erosion as affected by vegetation coverage. *Environmental Science* 6, 16-19. doi: 10.13227/j.hjlx.2000.06.004

Zhao, G., Mu, X., Jiao, J., An, Z., Klik, A., Wang, F., Jiao, F., Yue, X., Gao, P., Sun, W.,

544 2017. Evidence and causes of spatiotemporal changes in runoff and sediment yield
 545 on the Chinese Loess Plateau. *Land Degrad. Dev.* 28(2), 579-590. doi:
 546 10.1002/ldr.2534

547 Zhao, G., Mu, X., Tian, P., Wang, F., Gao, P., 2012. The variation trend of streamflow
 548 and sediment flux in the middle reaches of the Yellow River over the past 60 years
 549 and the influencing factors. *Resources Science* 34(6), 1070-1078.

550 Zheng, H., Miao, C., Kong, D., Wu, J., Zhou, R., 2020. Changes in maximum daily
 551 runoff depth and suspended sediment yield on the Loess Plateau, China. *J. Hydrol.*
 552 583. doi: 10.1016/j.jhydrol.2020.124611

553 Zheng, H., Miao, C., Wu, J., Lei, X., Liao, W., Li, H., 2019. Temporal and spatial
 554 variations in water discharge and sediment load on the Loess Plateau, China: A
 555 high-density study. *Sci. Total. Environ.* 666, 875-886. doi:
 556 10.1016/j.scitotenv.2019.02.246

557 Zheng, M., Cai, Q., Chen, H., 2007. Effect of vegetation on runoff-sediment yield
 558 relationship at different spatial scales in hilly areas of the Loess Plateau, North
 559 China. *Acta Ecologica Sinica* 27(9), 3572-3581. doi: 10.1016/S1872-
 560 2032(07)60075-4

Figure Captions

Fig. 1 Locations of 47 hydrological stations in the middle of the Loess Plateau, China.

Stations 1–9 are located in the eastern Helong section (left side of the main stream) of the Yellow River. Stations 10–30 are located in the western Helong section (right side of the main stream) of the Yellow River. Stations 31–37 are located in the Beiluo River basin, and Stations 38–47 are located in the Jing River basin.

Fig. 2 Example showing how the boundary lines at Station 31 are determined. Panels

(a) and (b) show the nonlinear upper and lower boundaries for Q in P1 and P2. Panels (c) and (f) depict the movement of the boundaries between P1 and P2. Panels (d) and (e) show the linear lower boundaries after logarithmic transformation of Q and SSC in P1 and P2. Note that the nonlinear boundaries in (a) and (b) indicate the stability of SSC with increasing Q , using relatively larger Q values and the related SSC values for fitting; whereas the linear boundaries in (d) and (e) emphasize the erosive ability of streamflow with low sediment loads, and they use medium Q values and their related SSC for fitting. Here medium Q values refer to those Q between two critical Q values, and the points with the smallest SSC show an almost linear relationship when Q is above one of the critical values; and SSC is relatively stable when Q is above another critical value.

Fig. 3 Contribution of total maximum- n -day-per-year SSL to total SSL during P1 and

P2 periods (contribution = Σ (sum of maximum- n -day-per-year SSL) / total SSL in P1 or P2), $n = 1$ (a), 2(b), 3(c), 4(d), 5(e), and 6(f). Each red point represents a value from a single station. Note that the maximum- n -days here are not necessarily

consecutive.

Fig. 4 Relationships between the contribution of maximum- n -day-per-year *SSL* to total *SSL* with control area for different hydrological stations during P1 (blue points, upper panels) and P2 (red points, lower panels). Panels (a–f) show the contributions of maximum-1-day to maximum-6-days *SSL* to total *SSL* with variable control area during P1. Panels (g–l) show the same as in (a–f) but for P2. Vertical dashed lines mark the control area of 10,000 km². Horizontal dashed lines mark an apparent threshold in the *SSL* percentage contribution for control areas above and below 10,000 km² in each graph.

Fig. 5 (a) Mean and (b) standard deviation of SSC/Q values, where $Q \geq 0.01$ m³/s, during P1 and P2 periods, at 47 stations (each red point represents the values at a single station).

Fig. 6 Changes in contributions of *SSC* to changes in *SSL* from P1 to P2. The box in the upper left corner of the figure displays the PDF curve of contributions of *SSC* at 47 hydrological stations. The contribution value is -46% at Station ID 34 and -2% at Station ID 3, and the negative value means the *SSC* may increase from P1 to P2, especially for small-to-medium discharges.

Fig. 7 $SSC-Q$ distributions during the P1 period for watersheds where gully landforms dominate the control area. Pink and black curves delineate the upper and lower boundaries of the data points. The captions correspond to station numbers in Fig. 1 and Table S1. The map at the bottom right summarizes how these boundary lines in the $SSC-Q$ graphs changed between P1 and P2 for stations across the region.

Fig. 8 Lower boundaries of data points from P1 after logarithmic transformation of Q and SSC for watersheds where gully landforms dominate the control area. The BEIE method is used to fit the red lines after removing data points with extremely large or small Q values. The bottom right inset map summarizes how these boundary lines in the graphs changed between P1 and P2 for stations across the region.

Fig. 9 Loess gullied-hilly landscape (right) and the processes by which SSC in flood events remains relatively stable at watershed scale in the wet season (left and middle).

Fig. 10 Land use on the Loess Plateau (a) in 1975 and (b) in 2015.

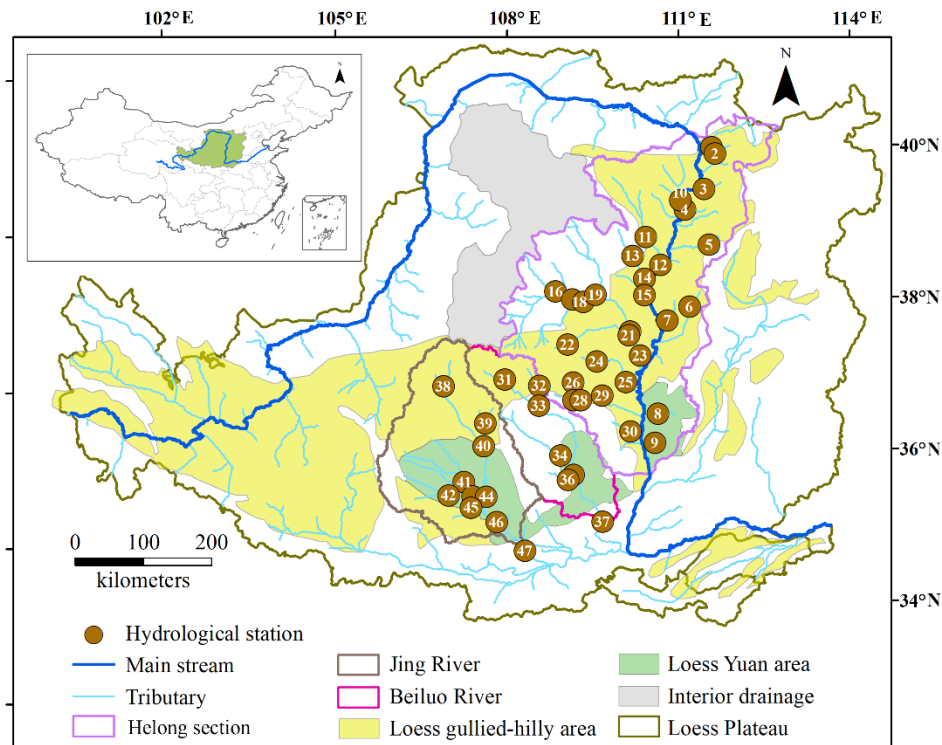


Fig. 1 Locations of 47 hydrological stations in the middle of the Loess Plateau, China.

Stations 1–9 are located in the eastern Helong section (left side of the main stream) of the Yellow River. Stations 10–30 are located in the western Helong section (right side of the main stream) of the Yellow River. Stations 31–37 are located in the Beiluo River basin, and Stations 38–47 are located in the Jing River basin.

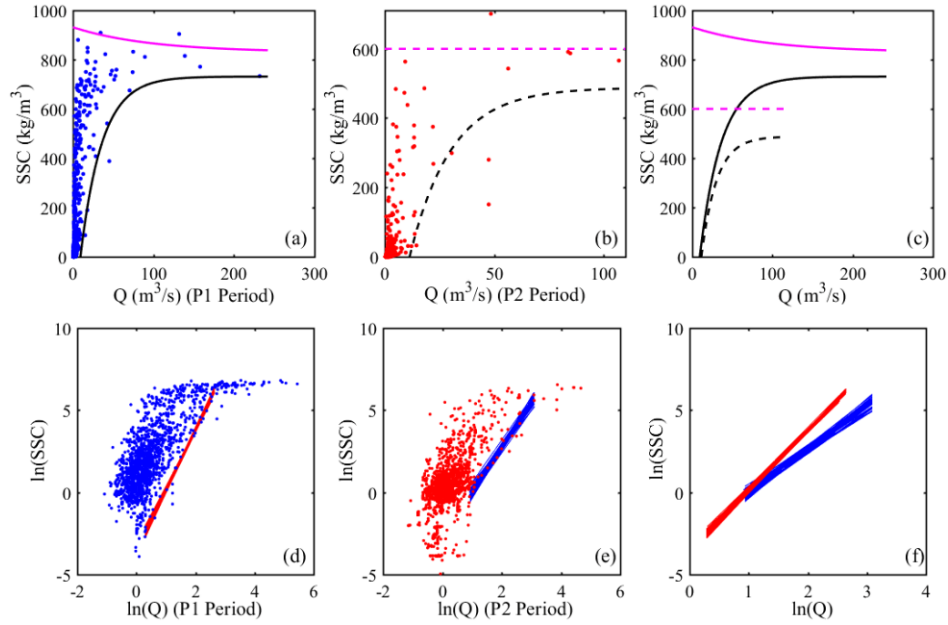


Fig. 2 Example showing how the boundary lines at Station 31 are determined. Panels (a) and (b) show the nonlinear upper and lower boundaries for Q in P1 and P2. Panels (c) and (f) depict the movement of the boundaries between P1 and P2. Panels (d) and (e) show the linear lower boundaries after logarithmic transformation of Q and SSC in P1 and P2. Note that the nonlinear boundaries in (a) and (b) indicate the stability of SSC with increasing Q , using relatively larger Q values and the related SSC values for fitting; whereas the linear boundaries in (d) and (e) emphasize the erosive ability of streamflow with low sediment loads, and they use medium Q values and their related SSC for fitting. Here medium Q values refer to those Q between two critical Q values, and the points with the smallest SSC show an almost linear relationship when Q is above one of the critical values; and SSC is relatively stable when Q is above another critical value.

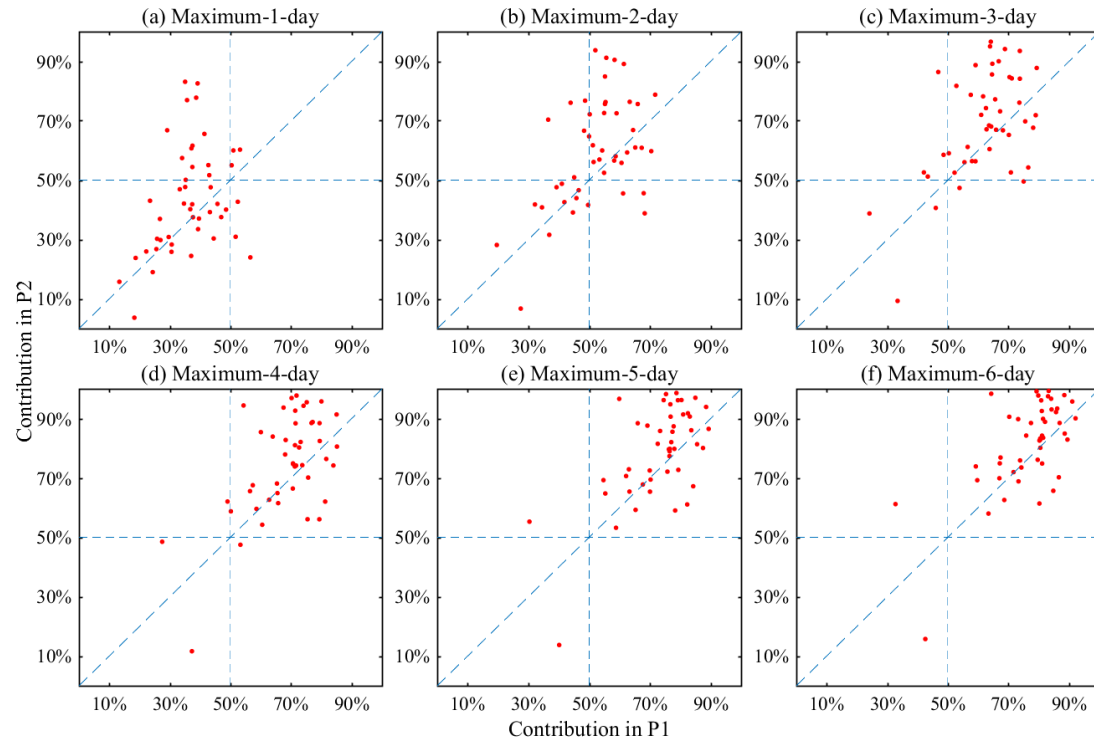


Fig. 3 Contribution of total maximum- n -day-per-year SSL to total SSL during P1 and P2 periods (contribution = Σ (sum of maximum- n -day-per-year SSL) / total SSL in P1 or P2), $n = 1$ (a), 2(b), 3(c), 4(d), 5(e), and 6(f). Each red point represents a value from a single station. Note that the maximum- n -days here are not necessarily consecutive.

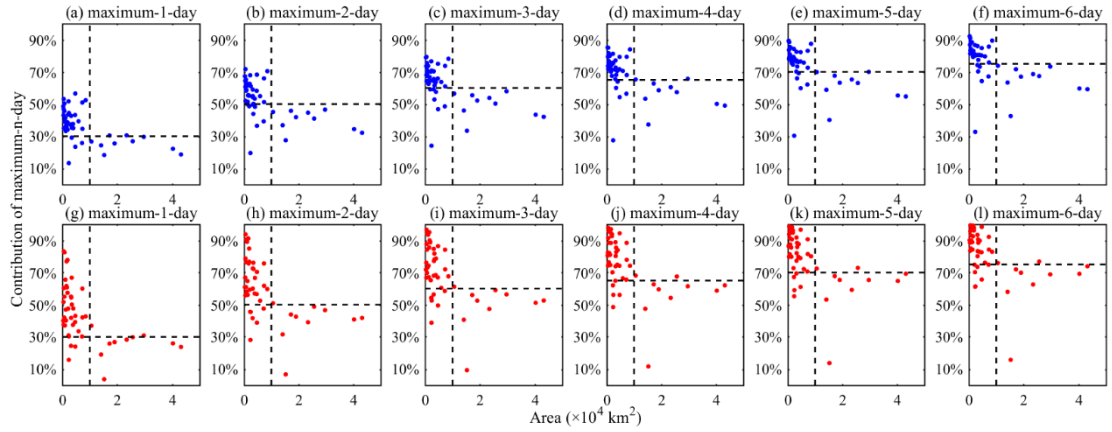


Fig. 4 Relationships between the contribution of maximum- n -day-per-year SSL to total SSL with control area for different hydrological stations during P1 (blue points, upper panels) and P2 (red points, lower panels). Panels (a–f) show the contributions of maximum-1-day to maximum-6-days SSL to total SSL with variable control area during P1. Panels (g–l) show the same as in (a–f) but for P2. Vertical dashed lines mark the control area of 10,000 km^2 . Horizontal dashed lines mark an apparent threshold in the SSL percentage contribution for control areas above and below 10,000 km^2 in each graph.

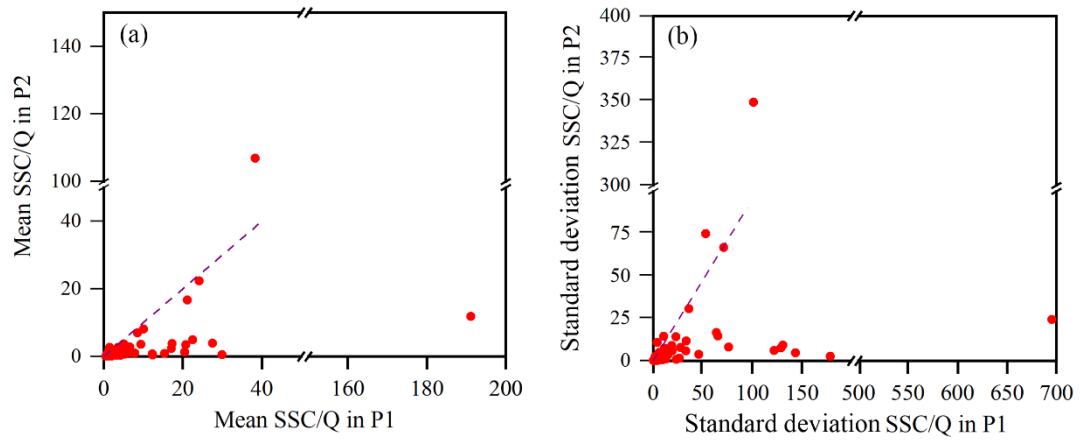
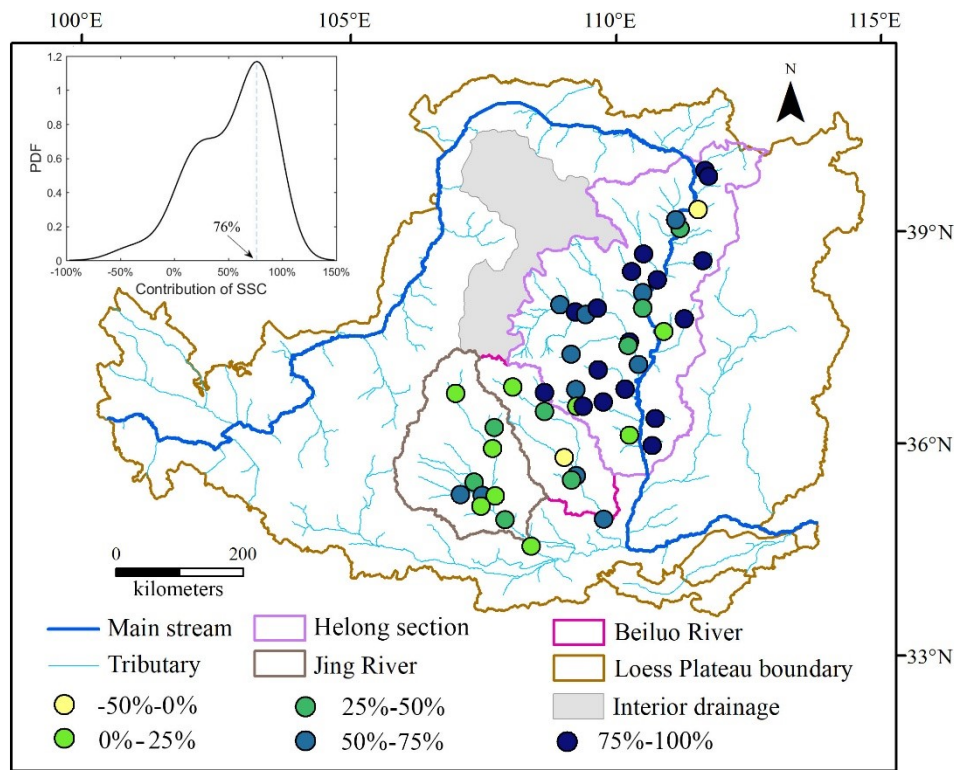


Fig. 5 (a) Mean and (b) standard deviation of SSC/Q values, where $Q \geq 0.01 \text{ m}^3/\text{s}$, during P1 and P2 periods, at 47 stations (each red point represents the values at a single station).

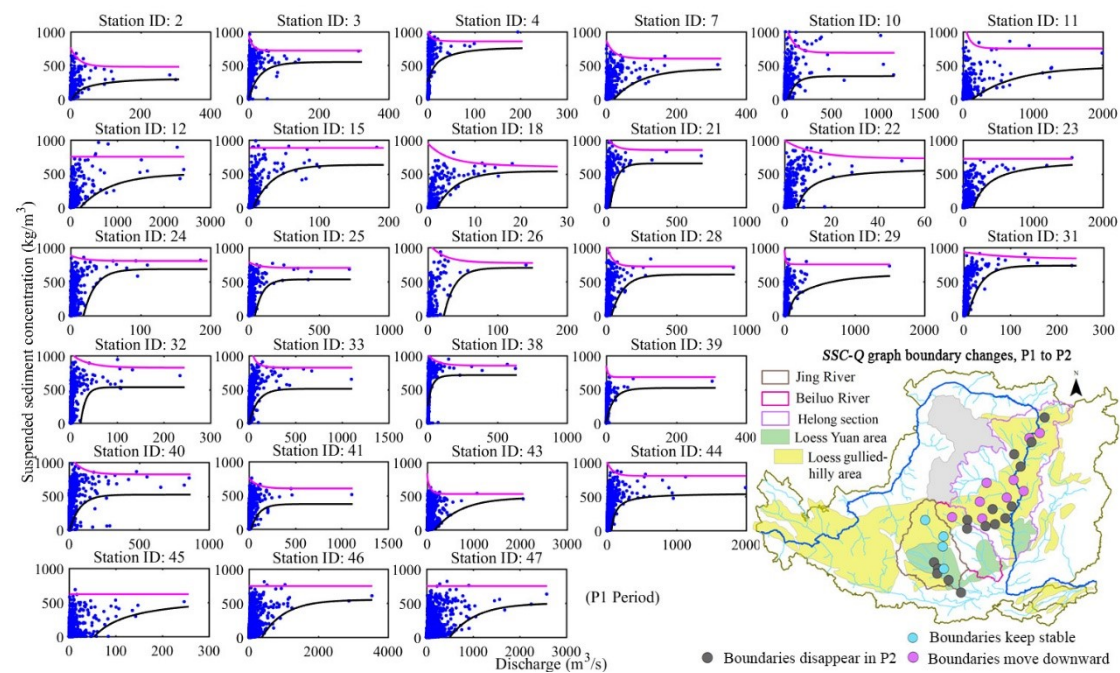


658

659 Fig. 6 Changes in the contributions of *SSC* to changes in *SSL* from P1 to P2. The box
660 in the upper left corner of the figure displays the PDF curve of contributions of *SSC* at
661 47 hydrological stations. The contribution value is -46% at Station ID 34 and -2% at
662 Station ID 3, and the negative value means the *SSC* may increase from P1 to P2,
663 especially for small-to-medium discharges.

664

665



666

667 Fig. 7 *SSC-Q* distributions during the P1 period for watersheds where gully landforms

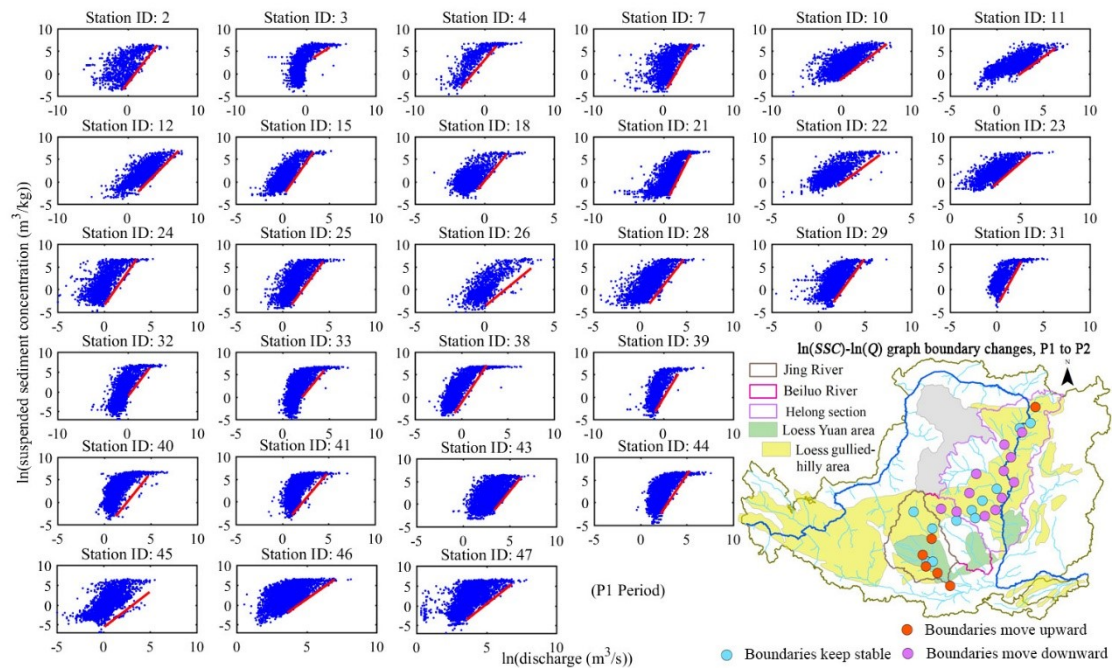
668 dominate the control area. Pink and black curves delineate the upper and lower

669 boundaries of the data points. The captions correspond to station numbers in Fig. 1 and

670 Table S1. The map at the bottom right summarizes how these boundary lines in the

671 *SSC-Q* graphs changed between P1 and P2 for stations across the region.

672



673

674 Fig. 8 Lower boundaries of data points from P1 after logarithmic transformation of Q

675 and SSC for watersheds where gully landforms dominate the control area. The BEIE

676 method is used to fit the red lines after removing data points with extremely large or

677 small Q values. The bottom right inset map summarizes how these boundary lines in

678 the graphs changed between P1 and P2 for stations across the region.

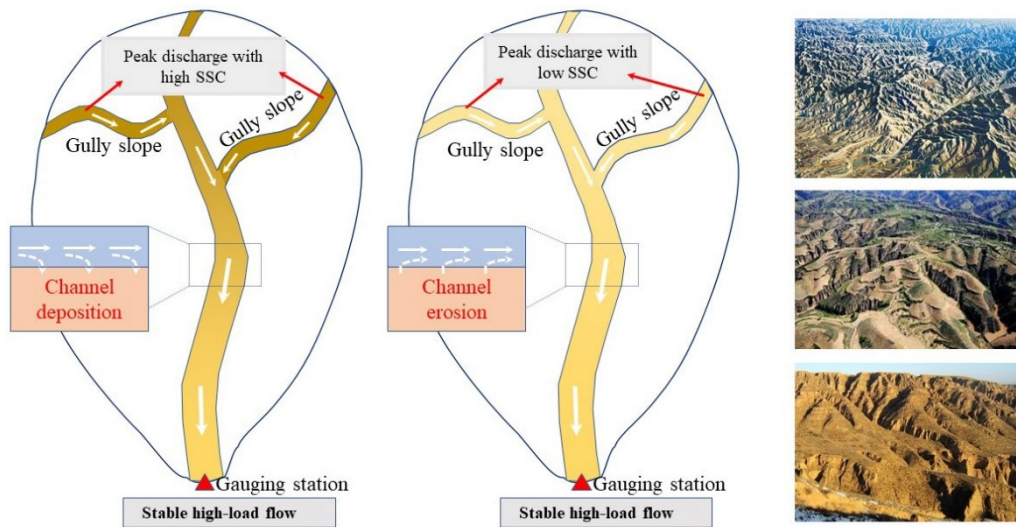


Fig. 9 Loess gullied-hilly landscape (right) and the processes by which *SSC* in flood events remains relatively stable at watershed scale in the wet season (left and middle).

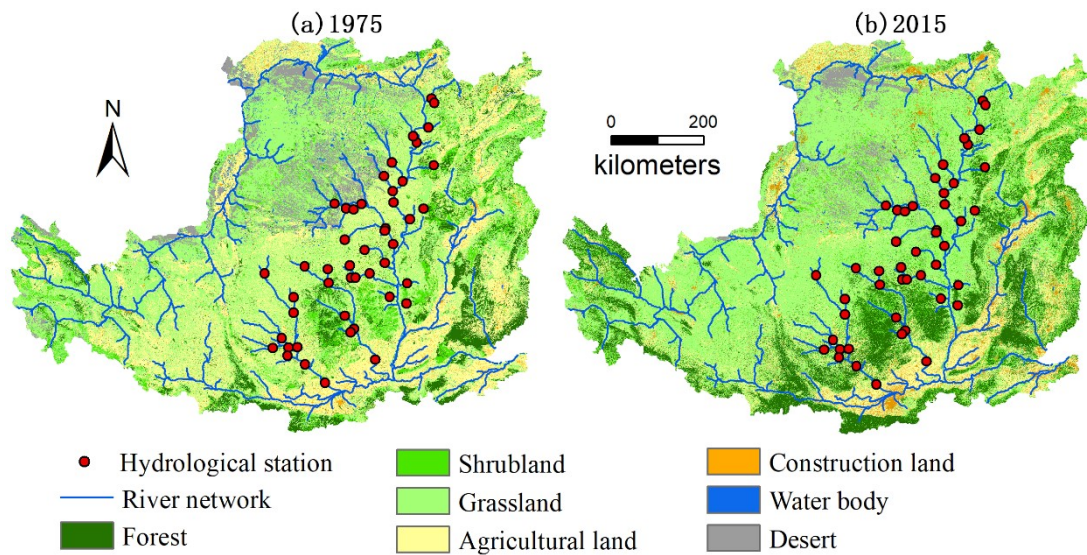


Fig. 10 Land use on the Loess Plateau (a) in 1975 and (b) in 2015.

685 *Supplementary Information for*

686 **Complex relationships between water discharge and sediment**
687 **concentrations across the Loess Plateau, China**

688

689

690 **Contents of this file**

691 **Table S1**

692 **Figs. S1-S8**

693

694 **Introduction**

695 This supplementary information section includes one table and eight figures that
696 support the results discussed in the main text.

Table S1. Locations of hydrological stations in Fig. 1.

Hydrological Station ID	Station Name	Latitude (°N)	Longitude		Control Area (km²)	Main Stream/	Type of Geomorphology
			(°E)			Subcatchment	
1	Dangyangqiao	39.98	111.62	4,732		Helong section (left side of main stream)	II
2	Qingshuihe	39.90	111.68	541		Helong section (left side of main stream)	I
3	Pianguan	39.43	111.48	1,896		Helong section (left side of main stream)	I
4	Jiuxian	39.16	111.16	1,562		Helong section (left side of main stream)	I
5	Kelan	38.70	111.57	474		Helong section (left side of main stream)	II

6	Gedong	37.88	111.23	749	Helong section (left side of main stream)	II
7	Linjiaping	37.70	110.87	1,873	Helong section (left side of main stream)	I
8	Daning	36.47	110.72	3,992	Helong section (left side of main stream)	II
9	Jixian	36.08	110.67	436	Helong section (left side of main stream)	II
10	Huangfu	39.28	111.08	3,175	Helong section (Huangfu River)	I
11	Shenmu	38.80	110.50	7,298	Helong section (Kuye River)	I
12	Wenjiachuan	38.43	110.75	8,515	Helong section	I

					(Kuye River)	
13	Gaojiapu	38.55	110.28	2,095	Helong section (Tuwei River)	II
14	Gaojiachuan	38.25	110.48	3,253	Helong section (Tuwei River)	II
15	Shenjiawan	38.03	110.48	1,121	Helong section (right side of main stream)	I
16	Hanjiamao	38.07	109.00	2,348	Helong section (Wuding River)	II
17	Hengshan	37.97	109.28	2,415	Helong section (Wuding River)	II
18	Dianshi	37.93	109.47	327	Helong section (Wuding River)	I

19	Zhaoshiyao	38.03	109.67	15,253	Helong section (Wuding River)	II
20	Dingjiagou	37.55	110.25	23,422	Helong section (Wuding River)	II
21	Suide	37.50	110.23	3,893	Helong section (Wuding River)	I
22	Qingyangcha	37.37	109.22	1,260	Helong section (Wuding River)	I
23	Baijiachuan	37.23	110.42	29,662	Helong section (Wuding River)	I
24	Zichang	37.15	109.70	913	Helong section (Qingjian River)	I
25	Yanchuan	36.88	110.18	3,468	Helong section	I

					(Qingjian River)	
26	Ansai	36.87	109.32	1,334	Helong section (Yan River)	I
27	Zaoyuan	36.63	109.33	719	Helong section (Yan River)	II
28	Yanan	36.63	109.45	3,208	Helong section (Yan River)	I
29	Ganguyi	36.70	109.80	5,891	Helong section (Yan River)	I
30	Xinshihe	36.23	110.27	1,662	Helong section (right side of main stream)	II
31	Wuqi	36.88	108.20	3,408	Beiluo River	I
32	Zhidan	36.82	108.77	774	Beiluo River	I

33	Liujiahe	36.55	108.77	7,325	Beiluo River	I
34	Zhangcunyi	35.90	109.13	4,715	Beiluo River	II
35	Jiaokouhe	35.65	109.35	17,180	Beiluo River	II
36	Huangling	35.58	109.27	2,266	Beiluo River	II
37	Zhuangtou	35.03	109.83	25,645	Beiluo River	II
38	Hongde	36.77	107.20	4,640	Jing River	I
39	Yuele	36.30	107.90	528	Jing River	I
40	Qingyang	36.00	107.88	10,603	Jing River	I
41	Maojiahe	35.52	107.58	7,189	Jing River	I
42	Jingchuan	35.33	107.35	3,145	Jing River	II
43	Yangjiaping	35.33	107.73	14,124	Jing River	I
44	Yuluoping	35.33	107.95	19,019	Jing River	I
45	Zhanghe	35.18	107.72	1,506	Jing River	I

46	Jingcun	35.00	108.13	40,281	Jing River	I
47	Zhangjiashan	34.63	108.60	43,216	Jing River	I

Note: Stations marked as Type I in the last column (29 stations) represent watersheds where most of the area (> 80%) is covered by the loess gully landscape; the exception is Baijiachuan station, where about half of the region is characterized by the loess gully landscape. Stations marked as Type II (18 stations) represent watersheds with complex, heterogeneous landscapes (the control areas include a combination of the loess gully landscape, desert, rocky mountain, etc.).

Table S2 Number of years in each station dataset for 47 stations along the Yellow River during P1 and P2

ID	P1	P2	ID	P1	P2	ID	P1	P2	ID	P1	P2	ID	P1	P2	ID	P1	P2
1	10	9	9	17	9	17	17	9	25	16	9	33	17	9	41	17	9
2	11	8	10	17	9	18	17	9	26	7	9	34	17	9	42	17	9
3	17	9	11	17	9	19	17	8	27	17	9	35	16	9	43	17	9
4	11	9	12	16	9	20	17	9	28	17	9	36	16	9	44	17	9
5	16	9	13	17	9	21	17	9	29	17	9	37	17	9	45	16	9
6	16	9	14	16	9	22	16	9	30	17	9	38	17	9	46	17	9
7	16	9	15	16	9	23	13	9	31	8	9	39	16	9	47	17	9
8	17	9	16	17	9	24	17	9	32	17	9	40	17	9			

The acronym ID corresponds to the hydrological station ID in Table S1.

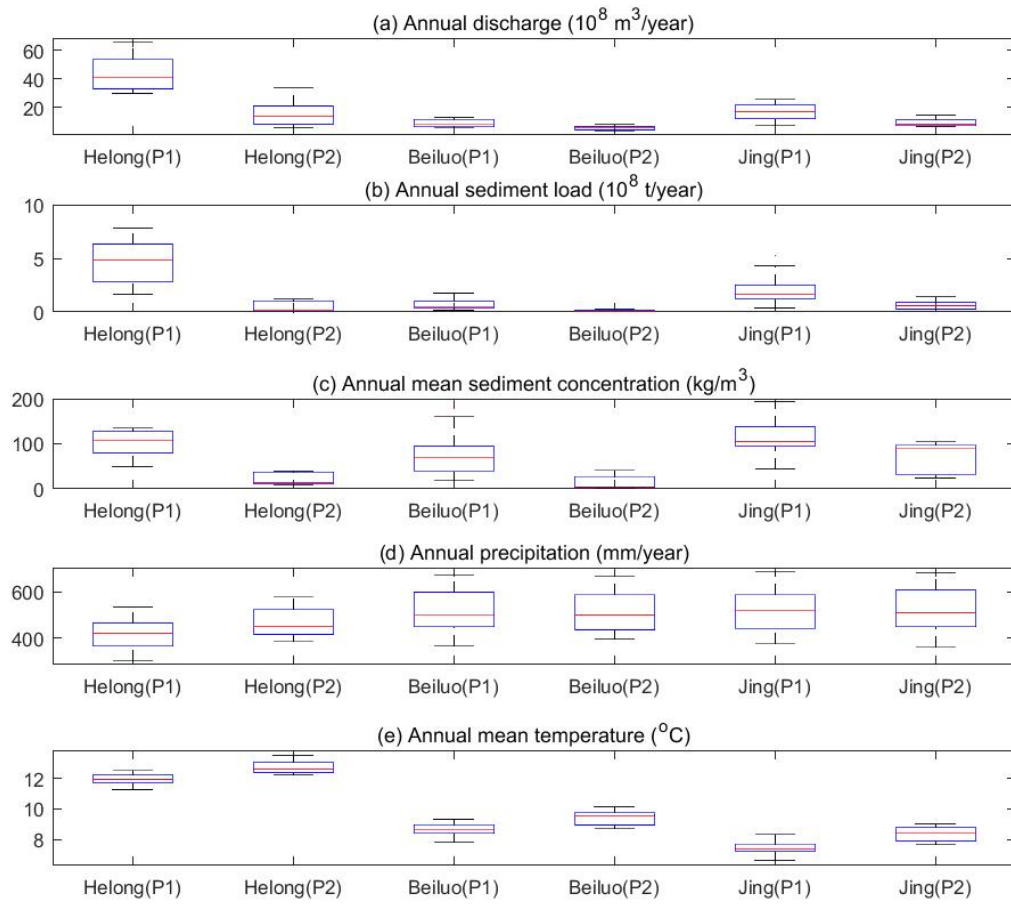


Fig. S1 Boxplots showing (a) discharge (Q), (b) sediment load (SSL), (c) annual mean sediment concentration (SSC), (d) annual precipitation (P), and (e) annual mean temperature (T) for the Helong section, Beiluo River, and Jing River during the P1 and P2 periods. The box plot is constructed from the minimum value, the first quartile, the median, the third quartile, and the maximum value. The P and T datasets are obtained from <http://data.cma.cn>. Note that the values of Q , SSL , and SSC for the Helong section are obtained as the difference between values at Longmen and Toudaoguai stations (both on the main stream of the Yellow River).

Uncertainties of the PDF-matching method

Step 1: Transformation of the PDF curves for Q during the P1 period to match the PDF curves obtained during P2, in order for the matched PDF for Q in P1 (Q') to be almost the same as the PDF for Q in P2. To check the effect of matching the PDF, we compare the mean annual Q' during P1 with mean annual Q during P2. Fig. S2 shows that the simulations are satisfactory at all the stations considered.

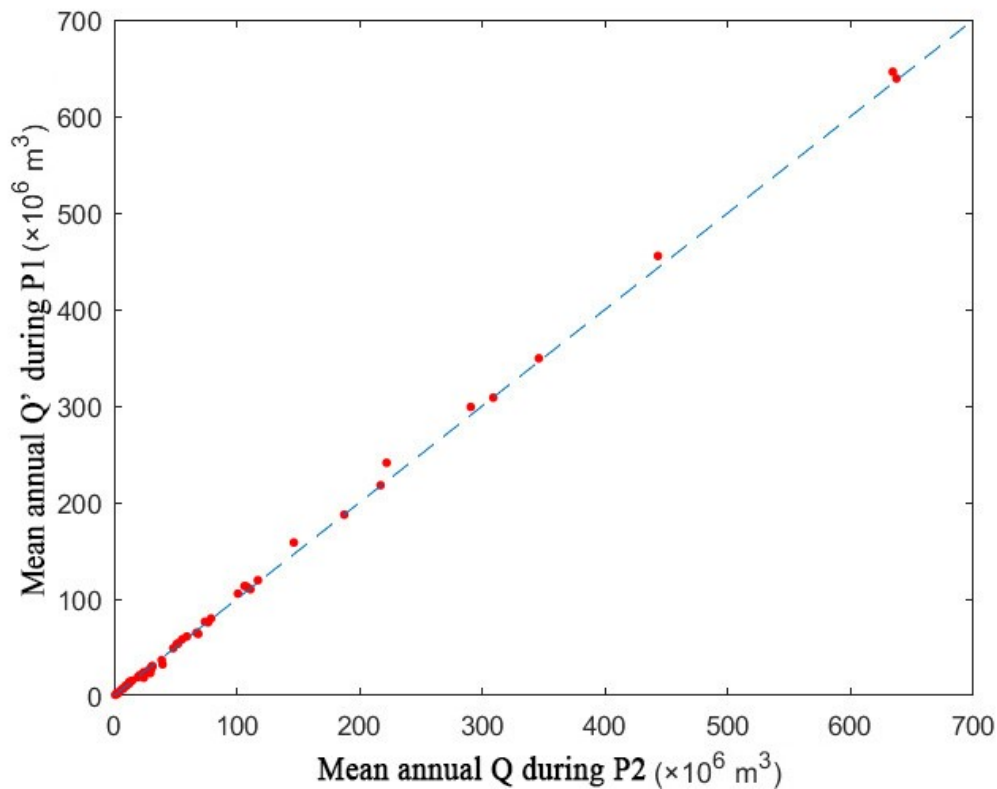


Fig. S2 Checking uncertainty in matching the PDF of Q to that of Q' .

Step 2: Calculation of the matched value of SSC for each interval (step length set to 3) of the observed Q in P1. For the few intervals without observed points, we use two interpolation procedures: 'Previous', where a null value is set equal to the value of a preceding interval; and 'Next' where a null value is set equal to the value of the next interval. Fig. S3 presents the results provided by these two methods, and it indicates

that there are hardly any differences evident for most stations, except at two stations where the data are particularly uneven.

In short, the results display close correlation between the amount of data and the uniformity of data distribution, with the ‘Next’ method better at handling very uneven data. We therefore selected the ‘Next’ interpolation method.

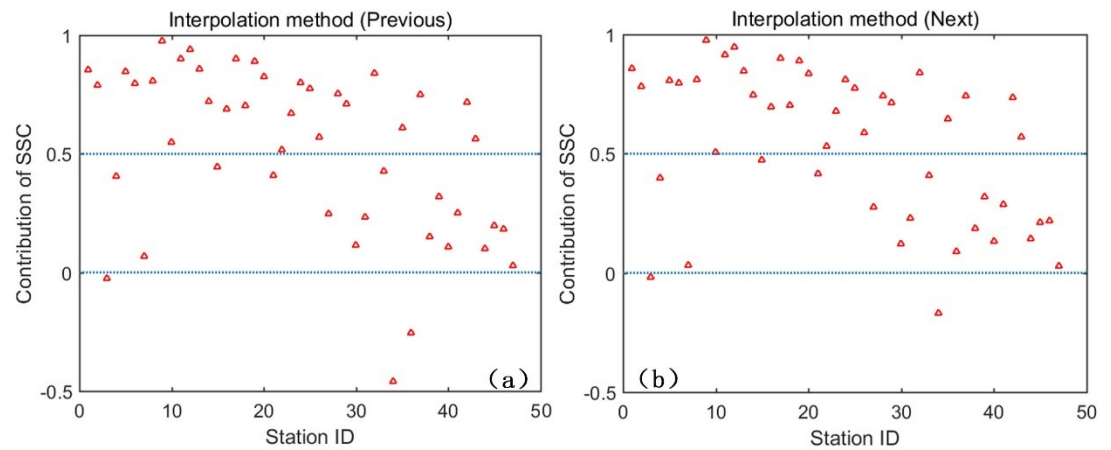


Fig. S3 Contribution of *SSC* to changes in *SSL* obtained using (a) “Previous” and (b) “Next” methods to fill null values.

Uncertainty analysis of ‘Boundary Estimation with Interval Extremum’ (BEIE)

To check the effect of sample size, we use bootstrap sampling (with drop-back sampling) to randomly pick 25, 50 and 75% of the prepared points to fit the boundary. It is clear from Figs S4 and Fig. 2 that sample size has a very important effect on the uncertainty of boundary fitting. It shows a thinner band of boundaries when picking 75% of the sample points than when picking 25% and 50% of the points. In addition, the distribution uniformity of points may also affect the fitting effect. For example, the method is not well suited for the observed $SSC-Q$ distribution because the majority of points are concentrated at small values and there is a huge difference between these points and the few points with large values. We use the method simply to obtain a rough boundary from the minority of points with larger values (Fig. 2a and b). But, as for log-transformed $SSC-Q$, the fitting boundaries are much improved, especially during P1.

In conclusion, attaining a higher degree of accuracy depends on having larger sample points and higher uniformity. In this study, the time series of the P2 data is not as long as that of the P1 data, which may lead to poorer boundary fitting in P2 than in P1. In practice, choice of step length (length = 0.2 in this study) has a great impact on the effectiveness of the fit. When the step size has a large value, the boundary can better encompass all data points; and when the step size has a small value, the influence of certain outliers can be eliminated.

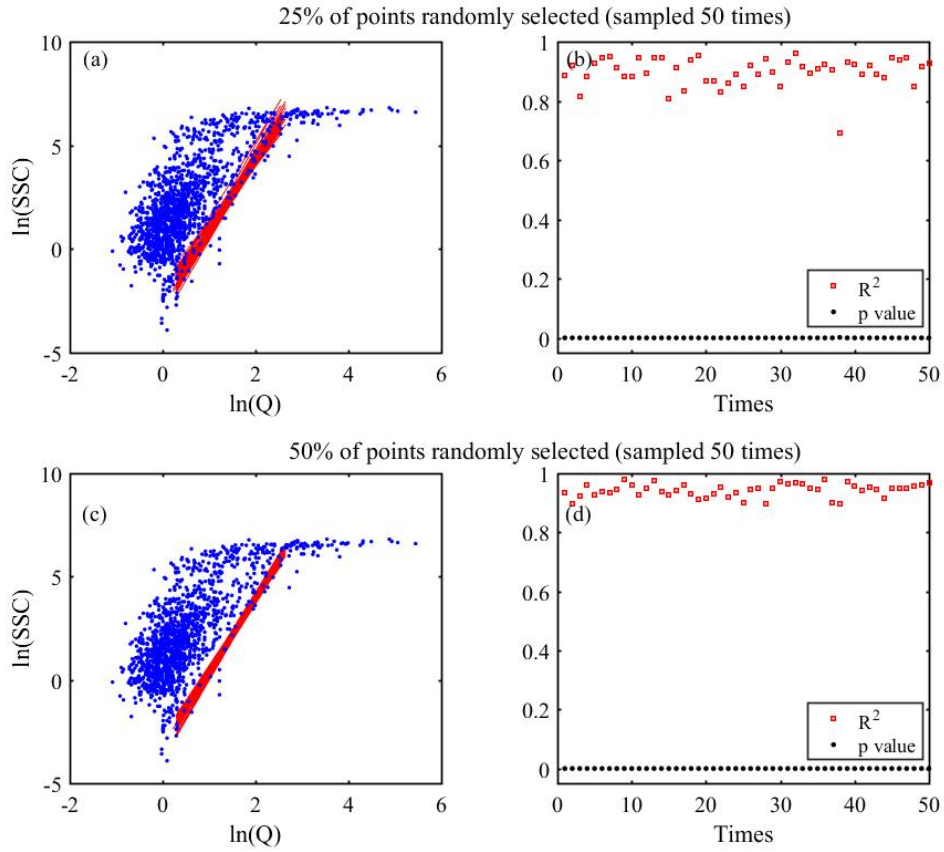


Fig. S4 The boundary fit obtained by randomly picking (a) 25% and (c) 50% of scatter-plot data points 50 times. Panels (b) and (d) show the R^2 and p values of these fitting boundaries and all p values < 0.01 in the figures.

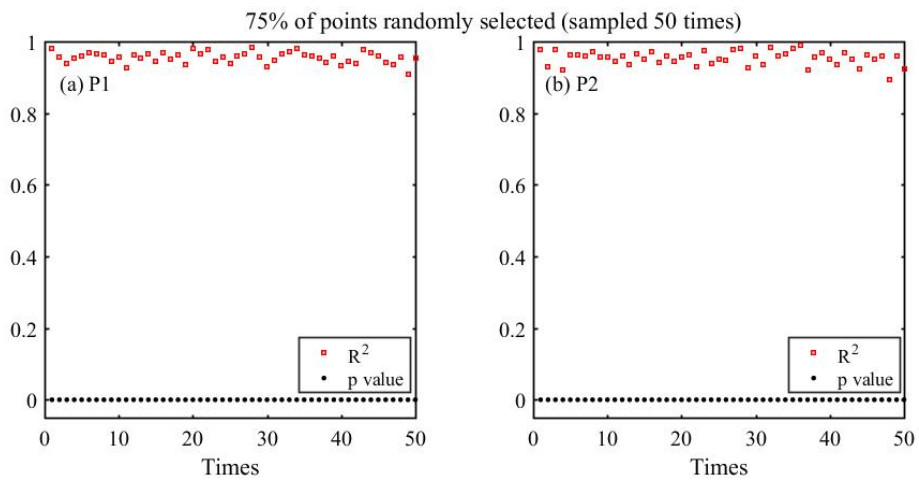


Fig. S5 R^2 and p values for line-fitting boundaries when randomly picking 75% of scatter-plot points in (a) P1 and (b) P2.

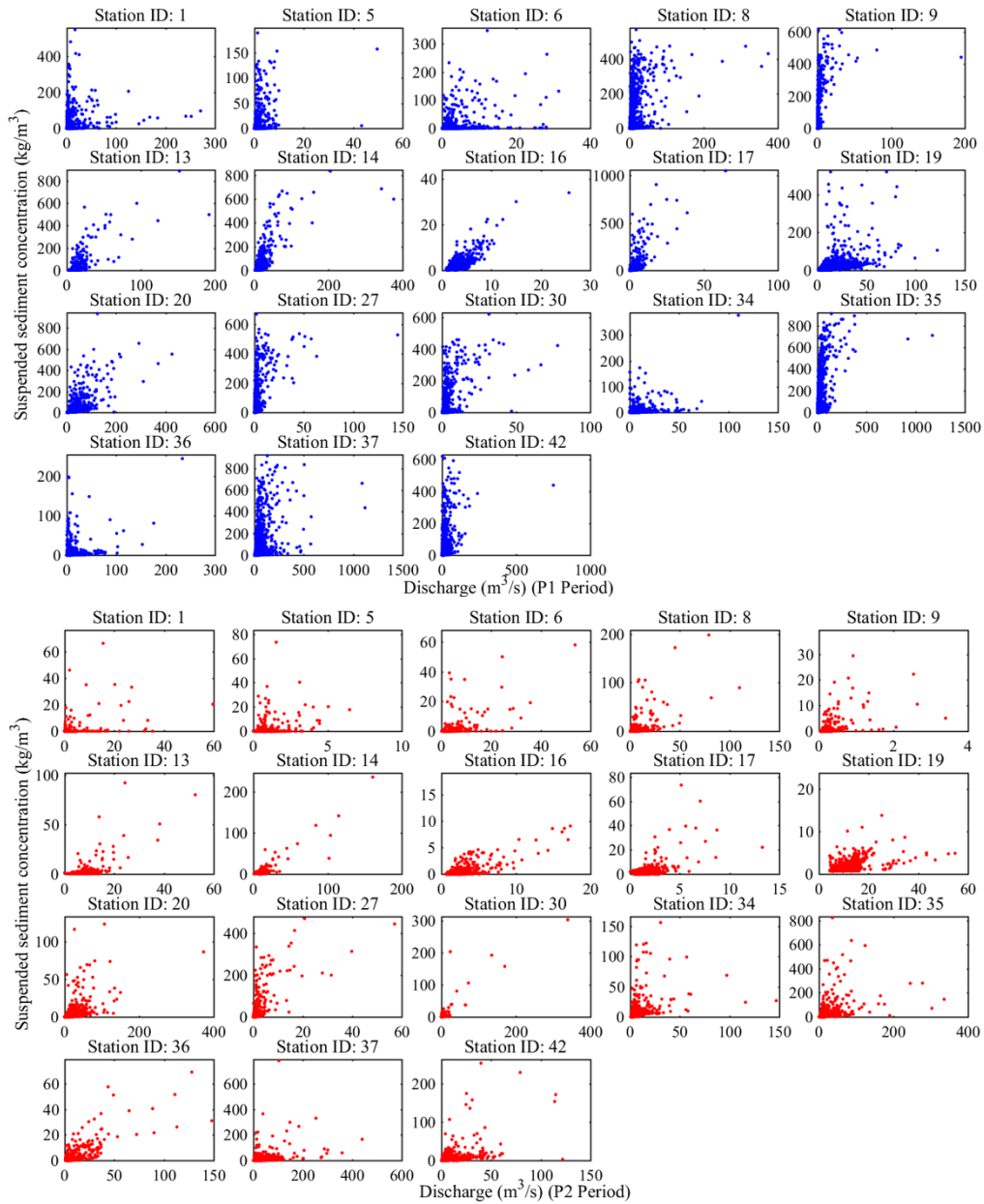


Fig. S6 SSC- Q distributions for watersheds with complex landscapes during P1 (blue dots) and P2 (red dots) periods.

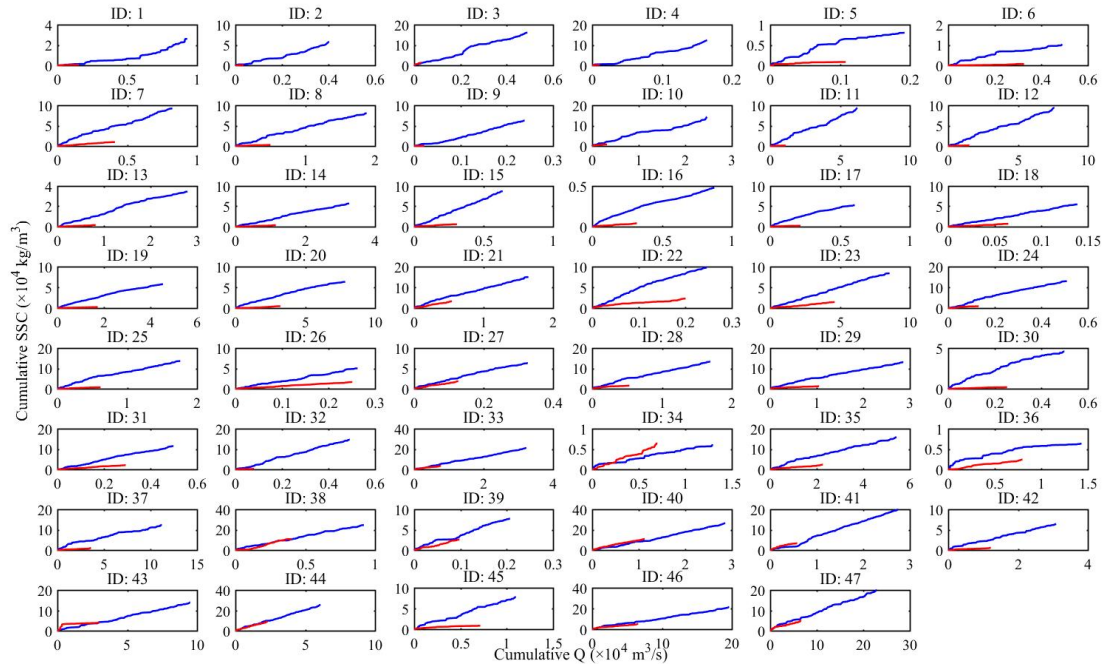
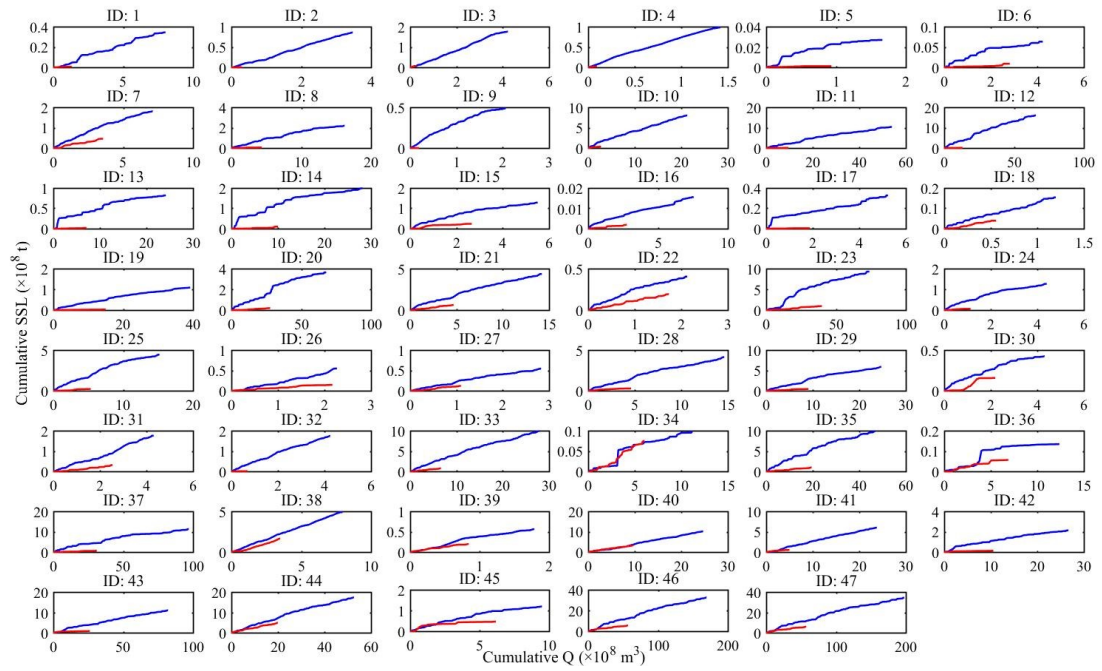


Fig. S7 Double mass curve relationships between cumulative Q and cumulative SSC for 47 stations along the Yellow River. Blue lines represent the relationship during P1, and red lines represent the relationship during P2. The number of years of available data for P1 and P2 for these stations is presented in table S2 (the observed data have missing values in certain years).

774



775

776 Fig. S8 Double mass curve relationships between cumulative Q and cumulative
777 sediment load (SSL) for 47 stations along the Yellow River. Blue lines represent the
778 relationship during P1, and red lines represent the relationship during P2. The number
779 of years of available data for P1 and P2 for these stations is presented in table S2 (the
780 observed data have missing values in certain years).